Accepted Manuscript

Analytical optimization of a nanoparticle of microstructural fused deposition of resins for additive manufacturing

Bankole I. Oladapo, A.O.M. Adeoye, Muhammad Ismail

PII: S1359-8368(18)30826-6

DOI: 10.1016/j.compositesb.2018.05.041

Reference: JCOMB 5711

To appear in: *Composites Part B*

Received Date: 13 March 2018

Accepted Date: 24 May 2018

Please cite this article as: Oladapo BI, Adeoye AOM, Ismail M, Analytical optimization of a nanoparticle of microstructural fused deposition of resins for additive manufacturing, *Composites Part B* (2018), doi: 10.1016/j.compositesb.2018.05.041.

Analytical optimization of a nanoparticle of microstructural fused deposition of resins for Additive Manufacturing

[a*]Bankole. I. Oladapo, [b]A. O. M. Adeoye, [c]Muhammad Ismail

[a]*Mechatronics and Mechanical Department, De-Montfort University, Leicester, UK*
[b]*Mechatronics Department, Afe Babalola University, Ado-Ekiti, Nigeria*
[c]*Department of Engineering, University of Leicester, Leicester, UK*
**Corresponding author, Tel: +44(0)1162013971, E-mail: P17243433@my365.dmu.ac.uk*

Abstract

The evolution of Additive manufacturing technologies (AMT) with Bioengineering production materials have been constantly researched, but not all have the necessary characteristics adequate fracture toughness to resist forces and crack propagation, with an improved mechanical and structural properties. The aim of this research was to analyse the nanoparticle microstructure and possible reinforcement of different resins behaviour to enhance productivities for ADT. Also to analyse the behaviour of different polymer resins in the attempt to make filaments for use in AMT, contributing to the sustainable search for natural resources of resins for 3D printing. Novel test analyses were carried out, which included mechanical evaluation of the materials for tensile and compression stress, density, glass transition temperature, Frequency analysis and optimization as well as the functional analytic behaviour of the samples with differential scanning calorimetry (DSC). The further analytical structural of the particle was performed, evaluating the surface luminance structure and the profile structure of a resin material in 3D printing, analysing the profile curve of the nanostructure from the scanning electron microscope (SEM). The filter profile of a cross-sectional view of the specimen was extracted and analyse and the Firestone curve of the Gaussian filter checking the roughness and waviness profile of the structure. According to the results, the materials present an in low tensile strength and compression, but excellent moulding to be extruded in the filaments and also injected. The resin sample B give a higher tensile and compressive force of about 365KN/m^2 and 650KN/m^2 respectively compare to others.

Keywords: 3D printing materials; resins; nanoparticle; Bioengineering materials; Filament; microstructure

1. Introduction

Additive manufacturing (AM) is a technology of constructing objects layer-by-layer based on computer-aided design (CAD) [1]. This technology attracts strong interest from both industry and academic in the field of bioengineering and others for the challenging possibility to build objects with complex shapes and minimal use of harmful chemicals at a reasonable speed [2, 3]. Additive manufacturing technology (AMT) that consists of creating a 3D object from a digital model. 3D printing technologies have evolved very rapidly in recent years beyond their traditional field of application [4]. In fact, 3D printing is widely used in a variety of manufacturing sectors ranging from the aerospace and automotive industries to Bioengineering [4, 5]. The various 3D printing technologies differ

in terms of cost, maximum spatial resolution and type of materials used. There are also relatively high costs of materials and equipment and the need for specialized personnel to operate it [6, 7]. The development of new materials like polyurea which is typical elastomer derived from the reaction product of an isocyanate component and a synthetic resin through a step-growth polymerization, and other polymers including the application of fillers in composites and could be a way to improve the mechanical properties of the components produced of FDM [6, 8]. On the other hand, the technique of fused deposition that recently became quite popular, especially among the non-specialized personnel, since it represents a very profitable approach for the production of 3D objects with a relatively good resolution [9]. The FDM consists of the layered deposition of the material to be printed by heating it, usually using this technique, the material for 3D printing is in the form of a filament, which may be polymerized, metal, ceramic, wood or even adhesive [10]. However, being a thermally driven process that requires the melting of a thermoplastic filament prior to the additive deposition of the extruded resource, it presents some limitations related to the materials to be deposited, since only a relatively small number of polymers have the thermal and rheological properties suitable to be easily processable through this technology [11, 12]. Currently, the most used plastics in 3D printing are derivatives of polylactic acid (PLA), acrylonitrile butadiene styrene (ABS), and polyethene terephthalate (PETG), Nylon, polyvinyl acetate (PVA) and polycarbonates, however, new materials come up every now and then. This represents a substantial opportunity for research into new renewable source materials for 3D printing [13, 14]. The aim of this work was to evaluate the behaviour of different polymer resins in the attempt to make filaments for use in 3D printing, contributing to the sustainable search for natural resources of resins for 3D printing. To have a new method analyses of the microstructure and nanoparticle of resigning, which included mechanical evaluation of the materials for tensile and compression stress, density, glass transition temperature. Frequency analysis and optimization as well as the functional analytic behaviour of the samples with DSC. Also to investigate the possible reinforcement of different resins and examine it nanoparticles and microstructural behaviour to enhance novel productivities for ADM

2. Methodology

The tested materials were commercially purchased, Benzoin (Styrax benzine) plant resins originating original from Singapore, Mirra (Commiphora myrrha) from Somalia and Olibanum (Boswellia papyrifera) from Ethiopia were purchased from Mountain Rose Herbs [15]. Its tensile and compression tests were performed using a universal test machine. The tensile and compression tests were performed in accordance with the standards to ISO 4287. The preparation of the test specimens was performed by placing the resins in silicone moulds already prepared in the normalized dimensions and curing the materials in an oven at temperatures between 90^{o}C and 105°C. The scanning electron microscope (SEM) samples were extracted from the centre of the specimen in the region of maximum deflection according to [16] as shown in Fig. 1. The SEM micrographs were taken of a reference specimen at temperature specimens tested at 200◦C. Fig. 1. Show a significant development of cavities in the resin bridges at 200^{o}C temperatures with more pores towards the centre due to a loss of the weight of the sample [17, 16]. Furthermore, the microstructure at high temperatures shows the presence of resin linkage between the individual nanoparticles. There is an overall material deformation in the analysis in Fig. 2. due to the internal damage that occurred in the resin.

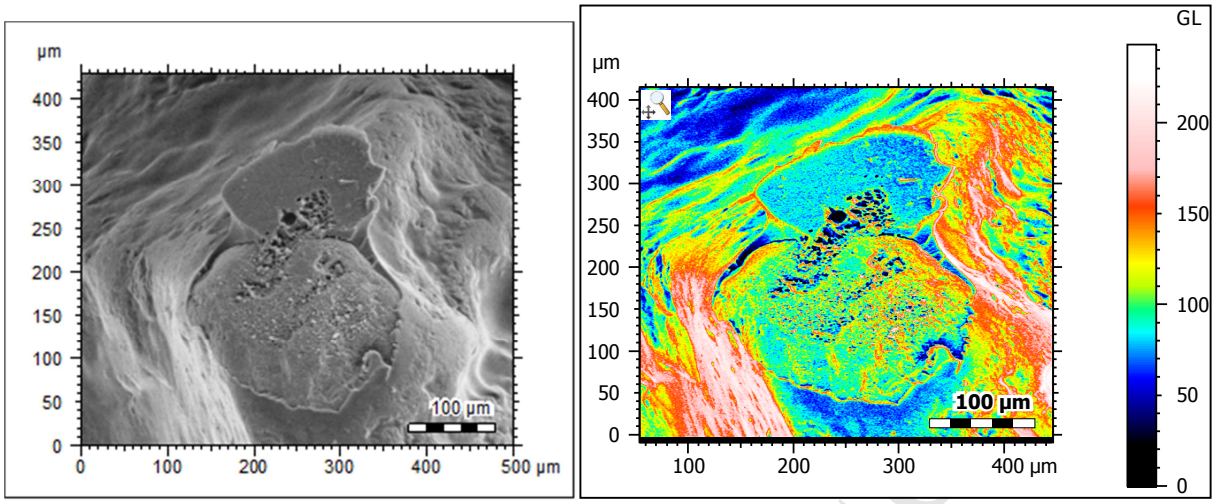

Fig. 1. SEM image of (a) resin bridges tested at 200◦C (b) luminance converted the view of the surface for analysis

ISO 4287 of the Resins				
Spacing parameters - Roughness profile				
RS	Nil	µm	Gaussian filter, 0.8 mm,	Mean width of the roughness profile elements.
Rdq	Nil	°	Gaussian filter, 0.8 mm	Root-mean-square of slope roughness profile.
Peak parameters - Roughness profile				
RPc	Nil	1/µ	Gaussian filter, 0.8 mm,	Peak count on the roughness profile.
Material Ratio parameters - Primary profile				
Pmr	0.16	%	c = 0.001 GL under the highest peak	The relative material ratio of the raw profile.
Pmr	0.16	%	c = 0.003 GL under the highest peak	The relative material ratio of the raw profile.
Pdc	65.8	GL	p = 20%, q = 80%	Raw profile section height difference.
Pdc	150	GL	p = 2%, q = 98%	Raw profile section height difference.
Amplitude parameters - Primary profile				
Pp	112	GL		The maximum peak height of the raw profile.
Pv	91.3	GL		Maximum valley depth of the raw profile.
Pz	203	GL		The maximum height of the raw profile.
Pc	67.0	GL	ISO 4287 w/o amendment 2	Mean height of the raw profile elements.
Pt	203	GL		The total height of raw profile.
Pa	31.9	GL		Arithmetic Mean Deviation of the raw profile.
Pq	38.7	GL		Root-mean-square (RMS) Deviation of the raw profile.
Psk	0.50			Skewness of the raw profile.
Pku	2.56			Kurtosis of the raw profile.
Amplitude parameters - Waviness profile				
Wp	33.6	GL	Gaussian filter, 0.25 mm	Maximum Peak Height of the waviness profile.
Wv	10.8	GL	Gaussian filter, 0.25 mm	Maximum Valley Depth of the waviness profile.

Wz	44.4	GL	Gaussian filter, 0.25 mm	Maximum Height of waviness profile.
Wc	Nil	GL	Gaussian filter, 0.25 mm, ISO 4287 w/o	Mean height of the waviness profile elements.
Wt	44.4	GL	Gaussian filter, 0.25 mm	Total Height of waviness profile.
Wa	11.0	GL	Gaussian filter, 0.25 mm	Arithmetic Mean Deviation of the waviness profile.
Wq	13.5	GL	Gaussian filter, 0.25 mm	Root-mean-square (RMS) Deviation of the waviness
Ws	1.22		Gaussian filter, 0.25 mm	Skewness of the waviness profile.
Wk	3.12		Gaussian filter, 0.25 mm	Kurtosis of the waviness profile.

2.1. Determination of setting of the resin sample test

In the material density test, 1 g of each material was analyzed using a digital densimeter (Gehaka DSL910) with precision from 0g/cm^3 to 3g/cm^3. The tests were performed in accordance with ASTM D792 (2013) specific for plastics. The glass transition point (Tg) of a solid is the temperature at which material changes from solid to liquid at atmospheric pressure. According to ASTM E 114207, the glass transition temperature is defined as a temperature chosen to represent the temperature range over which Tg occurs [18, 19]. In the tests, the grain-shaped materials were placed inside a 1L becker and this was placed inside a pump with internal pump circulation and temperature control. The Tg point was determined by visually verifying the occurrence of the denting with a consequent transition from the solid state to the viscous liquid state, the evaluation of the temperature within the becker was performed using a digital thermometer [12, 20]. The samples were weighed (2.0mg ± 0.5mg), and hermetically sealed in porcelain crucibles and placed in a Shimadzu calorimeter, model DSC60, in a nitrogen atmosphere, with a flow of 50 mL min1, in the heating ratio of 20°C min1 until reaching the maximum temperature set at 550 ° C. The equipment was calibrated in relation to temperature with the Indian standard (156.6 ° C ± 0.3) through its melting peak. The heat flux and enthalpy was calibrated through the Indian heat of fusion (28.59 J / g ± 0.30) using the same conditions of the samples. The correction factor was calculated according to Shimadzu's procedures and specifications [21, 22]. The extrusion tests, a screw extruder with polymer grain feed tray and filament outlet of 1.75 mm was used. The powdered resins were added to the feed hopper of the extruder and then the material was heated to near its glass transition temperature (65-95°C) [23, 24]. Upon cooling to room temperature (20øC) the materials solidified, thus obtaining solid filaments having the dimensions 30 cm long x 0.7 circular section. Extrusion speed was maintained at 10 mm/s. The extrusion control was performed by means of a step motor controller board and heating was performed by induction directly on the central tube body [18, 2]. In order to carry out the tests, ISO 5272 (2012) was consulted. For the print tests, a hotend with integrated cooler and temperature control, commercially available, was used, the equipment was connected to a 12V, 9A source. The unit has a filament inlet of 1.75 mm and the outlet of the heater head is 0.4 mm. The tests were performed in accordance with ASTM D3641 (2015). According to [8, 25]the variance (σ²) of the image sample is calculated as follows:

$$Variance = \sigma^2 = \frac{1}{N}\sum_{I=1}^{N}(x_i - \mu)^2 \quad (1)$$

where σ² = population variance of the sample resine, x_i = the ith parameter's value (or observation), μ = the

arithmetic mean of all observations and N = total number of observations in the population. And the stardand daviation is the square root of the variance of image according to equation 2

$$Stardand\ Deviation = \sqrt{Variance} = \sqrt{\sigma^2} = \sqrt{\frac{1}{N}\sum_{l=1}^{N}(x_i - \mu)^2} \quad (2)$$

According to Fig. 2a. Analytical luminance motifs for resins specimen was carried out with a 778 number of motifs mode in a standard area of 227µm² with area standard deviation of 444µm² and lower and upper quartile of 67.6µm² and 293µm² respectively

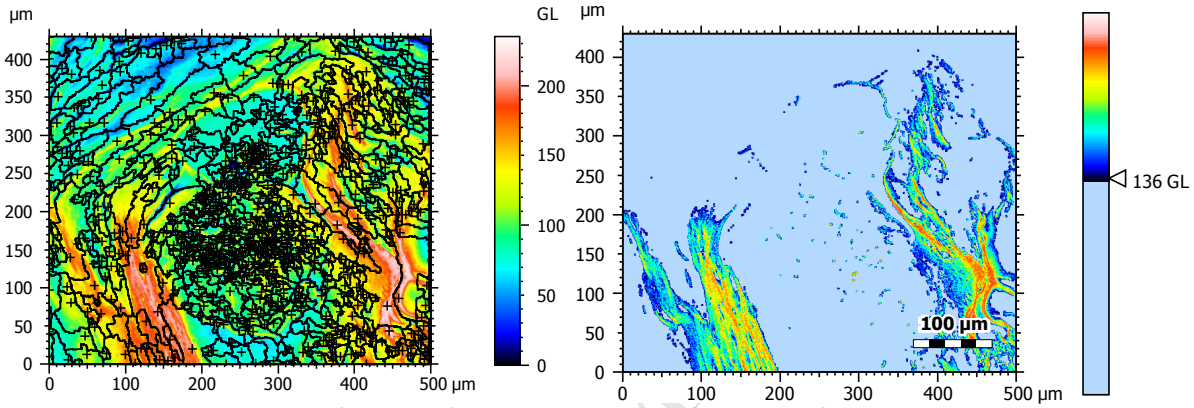

Fig. 2 Analytical parameter of the resin for (a) Luminance motifs analysis of resins (a) Luminance volumetric analysis of the resins

The mean height of the settings for the test is 23 with lower and upper quartile of 14.9 and 26.7 respectively, of a pitch diameter of 21µm and pitch standard deviation of 15µm. The mean form factor of the test is 0.512 of the standard deviation of 0.145 according to equation 1, with lower and upper quartile of 0.407 and 0.622 respectively with a form factor variance of 0.0211. The mean aspect ratio is 3.01 of the standard deviation of 3.83 and compactness for of the resin materials to be 0.667. Fig 2b represent the volumetric island of the sample of mean area of 187µm² at a maximum orientation angle of 58.5^{o} settings of an equivalent diameter of 5.19µm which has a maximum angle of -22.3^{o} and a minimum angle of -8.94^{o} with an aspect ratio of 2.99. This where the setting and the condition at which the test was carried out.

3. Results and discussion

Fig. 3 presents the results of the tensile and compression tests. The resins were identified as follows: Boswellia papyrifera (resin A), Styrax benzoin (resin B) and Commiphora myrrha (resin C). According to the results presented in fig. 3a and 3b, resin B reached the highest values of tensile strength as well as compression. The brittleness of the materials due to their high crystallinity is an aspect that must be taken into consideration during the tests, as it made testing difficult in general.

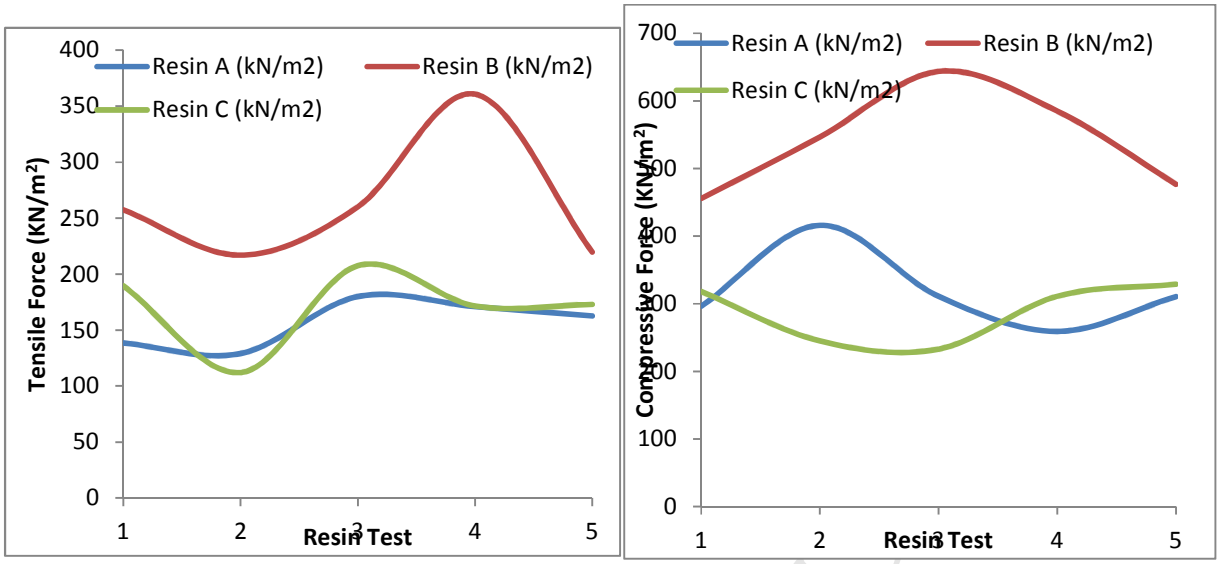

Fig. 3 Results for (a) tensile force test and (b) compression force tests of the resins specimens

From fig. 3a and 3b the optimum tensile and compressive can be observed in resin B at approximately 360KN/m^2 and 650KN/m^2 respectively. This is due to the temperature of preparation of the specimens which was maintained between 70^{o}C to 95°C, so that the materials showed crystalline glassy behaviour [26, 11], with rigid and fragile behaviour. These values can be considered low if compared to the temperatures that other commercial plastics can withstand, but these values may increase with the addition of fillers or plasticizers, or even with the change in the temperatures used in the confirmation of the specimens.

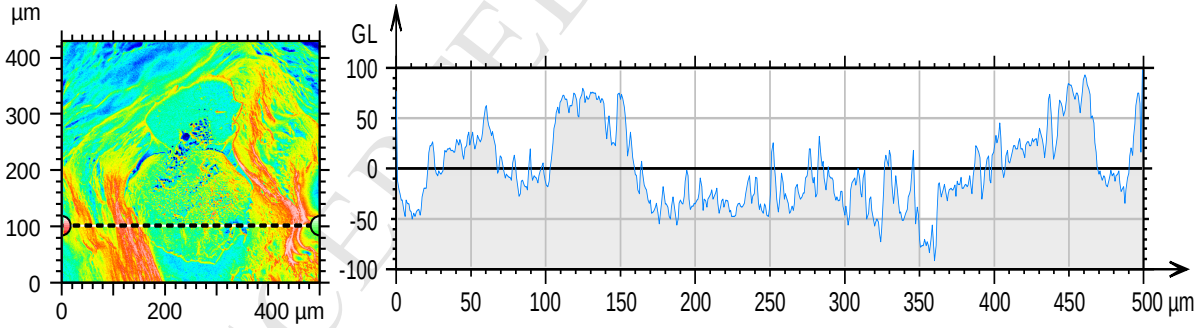

Fig. 4. Extraction profile curve at 100 µm level across the 500 µm of the resin structure

One option would be to prepare the specimens for tensile and compression tests using the FDM 3D printing technique, controlling the temperature and quantity of material to be deposited per layer, instead of using models for this purpose [27, 10]. Fig. 5a represent extraction profile curve and the histogram of abbot-firestone of the Gaussian filter of setting to 250µm of roughness and waviness profile of the resins in 3D printing. The scale in depth of the abbot-firestone is calibrated at 100% of the relative material ratio of the profile (Pmr) where (c) is the highest peak of the material profile. The different in c1 and c2 is 43.9GL and the difference in Pmr(c1) and Pmr(c2) is 9.36%.

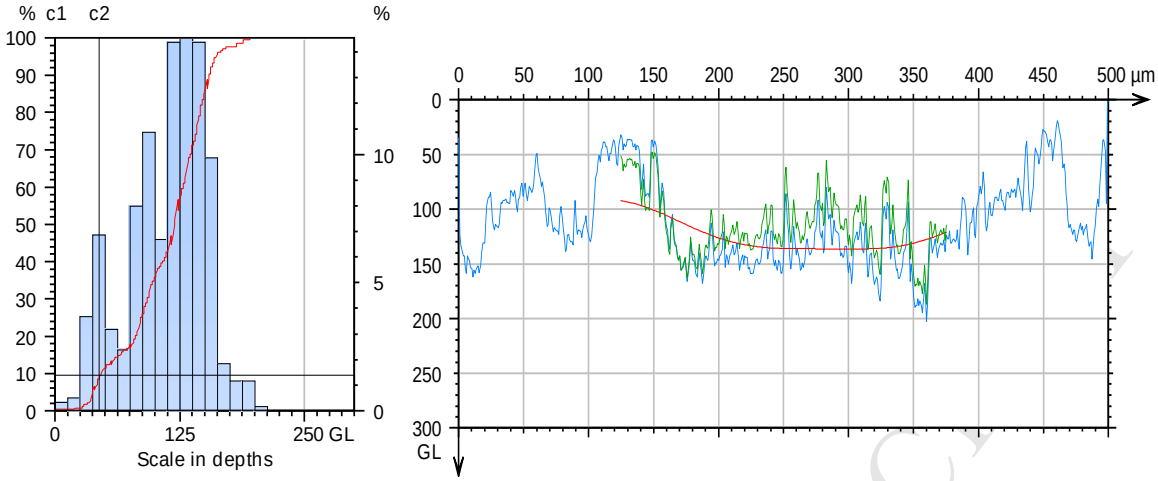

Fig. 5 Extraction profile curve of (a) Histogramme and abbot-firestone curve of the Gaussian filter of setting to 250µm (B) Roughness and waviness profile of according to (a) of the resins in 3D printing

As regards the extrusion and filament tests, the materials presented similar behaviour, however, the test temperatures were different due to the intrinsic properties of the resins. In view of the temperatures set forth in Table 2, which are indicated in the analyzed materials, it can be noted that they are slightly below the temperatures commonly used to print other materials usually employed in 3D printing technology. According to [28, 4] the printing temperature of PLA material is commonly performed between 190^{o}C and 220°C and the heating table in which the material is deposited should be maintained between 23^{o}C and 60°C. For example, the ideal extrusion temperature of 1.75 mm ABS plastic is 230°C and the table should remain at least 100^{o}C to 110°C throughout the print to ensure the workpiece adheres. According to [28, 29] recommendations for printing materials such as Polycarbonate and Nylon in general, it is necessary to reach temperatures around 260°C, so it is important to check the characteristics and limitations of the printer to avoid permanently damaging the hot-end head which may not withstand temperatures above 250°C [30, 31]. According to the manufacturer of filaments and printers M3D (2016), plastics such as PLA and ABS are quite resistant to mechanical stress, but have high contraction coefficients of 14mm, which makes it difficult to print larger parts that tend to deform (Warp effect), cracking and peeling off the table during printing [32, 15]. It is important to emphasize that it is still necessary to perform thermal expansion and contraction tests for the resins evaluated in this study. In the tests of extrusion and printing, it was verified that the cooling of the materials can be carried out at room temperature 20°C [33] without the need for heating of table and artificial refrigeration, because the materials solidify naturally, due to their intrinsic characteristics. It should be noted that parameters such as temperature and injection speed need to be optimized for better resolution. It is also worth mentioning that the filaments produced were not reel-wound because they still exhibited fragile and brittle behaviour, so in the tests, the filaments were printed in the shape of rods. Table 2 presents the results of the density and glass transition temperature (Tg) tests for the materials tested.

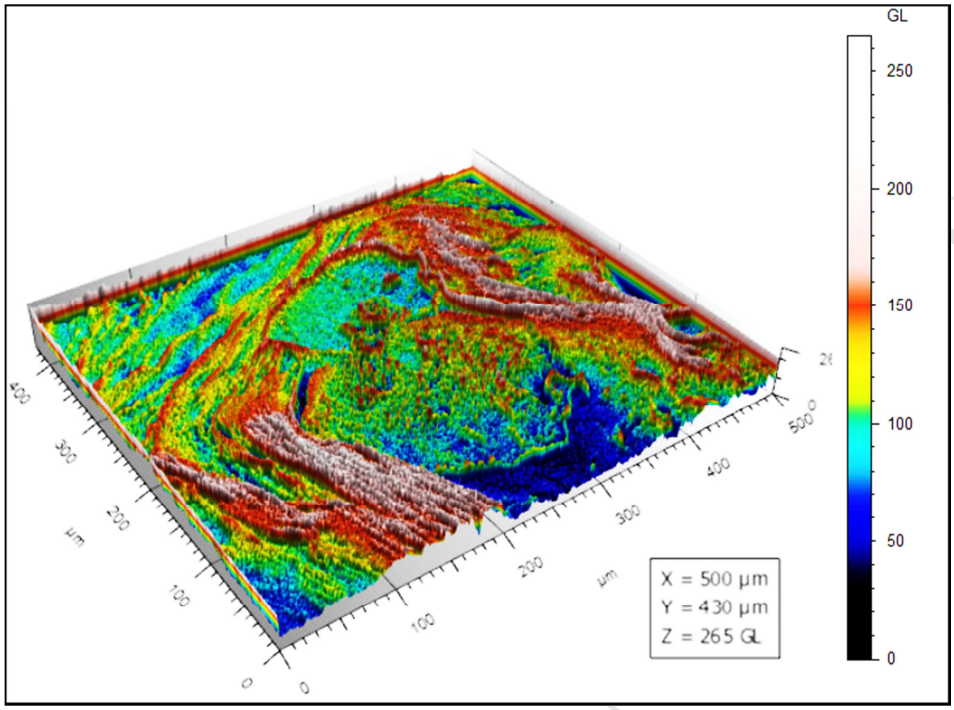

Fig. 6 The surfaces 3D view of the level least square method of the specimen

Table 2 Density and glass transition temperature of materials

Materials	Glass transition Temperature Tg (^{o}C)	Density (Kg/m3)
Resine A	78	1250
Resine B	95	1310
Resine C	89	1020
PLA	60	1240
ABS	105	1030
PETG	88	1270

According to Table 2 the resins tested in this work presented approximate Tg to the other commercial plastics. In the same table, the results concerning Tg temperature and density values for the other plastics. 95°C, followed by the consequent mass loss of the material after reaching 95°C and denotes that the glass transition temperature for this resin actually occurs from 95°C to 270°C, so at this temperature range the material is presented as a mobile liquid, in this condition the behaviour of this polymer is rigid and fragile, since the polymer chains do not have enough energy to have mobility, preferably responding in an elastic way to the requests [34, 35]. At about 280 ° C, the occurrence of an initial crystallization band is observed through the phase change and the strong exothermic peak. At about 400°C, another crystallization peak is observed. In this phase the material presents a rubbery behaviour, the energy level is enough to give mobility only the amorphous phase, keeping the crystalline phase rigid. At about 500°C the

material exhibits viscous behaviour, and a third exothermic peak around 510°C thus indicates its melting temperature, at which point the resin exhibits molten behaviour [36, 36]. This high energy level is characterized by having highly mobile polymer chains. Fig. 7a is the Fractal analysis of fractal dimension 2.55 with the morphological envelops methodology. The first slope value is 0.45 and the second is 0.261 of the regression $(R_1)^2$ and $(R_2)^2$ of 0.996 and 0.995 respectively on a scale analysis. The optimum values according to the two slopes of the line as shown in Fig. 7a is at the 32µm on the scale analysis and 3000µm^3 of an enclosed volume. Fig. 7b shows the peak count distribution histogram of grains in a micrometre cube of luminance for differential scanning calorimetric of resins.

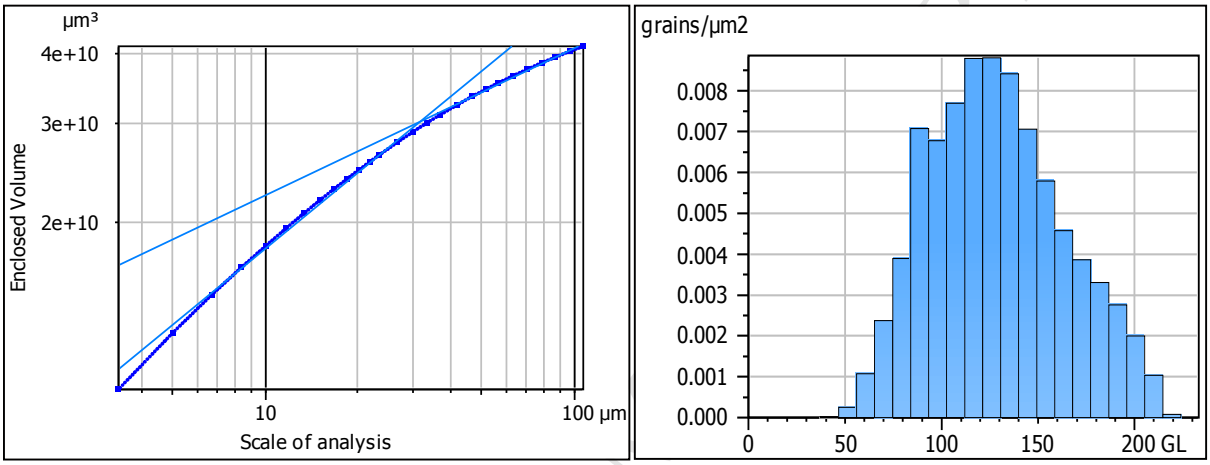

Fig. 7 The resins sample grain of luminance of (a) Fractal analysis of fractal dimension 2.55 with morphological envelops method (b) Peak count distribution histogram of grains luminance for differential scanning calorimetric of resins

The analytical domain of the scale of sensitivity analysis and the regression settings of the system was done automatically at a smooth-rough crossover (SRC) threshold of 10%. The luminance scale sensitivity analysis of complexity scale area of one corner of the resins sample is shown in Fig. 8a A area scale of one corner methodology was used of an SRC of 3054µm² and an SRC threshold of 537. It has a fractal complexity of 191 on a number of points of 40 and a fractional dimension of 2.38 with a maximum scale complexity of 6857 µm² of heterogeneity complexity of 153,251 according to Fig. 8a generated from the experiment. The regression coefficient of the 'R' square equation is 0.988 while the regression line is at the 8000µm². Also the analytical domain of the scale of sensitivity analysis and the regression settings of the system was done automatically for the four corner analysis at an SRC threshold of the same 10% of the resins sample which is shown in Fig. 8b A area scale of one corner methodology was used of an SRC of 2451µm² and an SRC threshold of 558 [37, 38]. It has a fractal complexity of 171 on the same number of point 40 as that of one corner methodology. It has a fractional dimension of 2.38 with a maximum scale complexity of 2597µm² which is about 37.87% to that of one corner methodology of the same heterogeneity complexity of 153,251 according to Fig. 7b generated from the experiment. The regression coefficient of the 'R' square equation is 0.997 while the regression line is at the 2600µm² as shown in Fig. 8b.

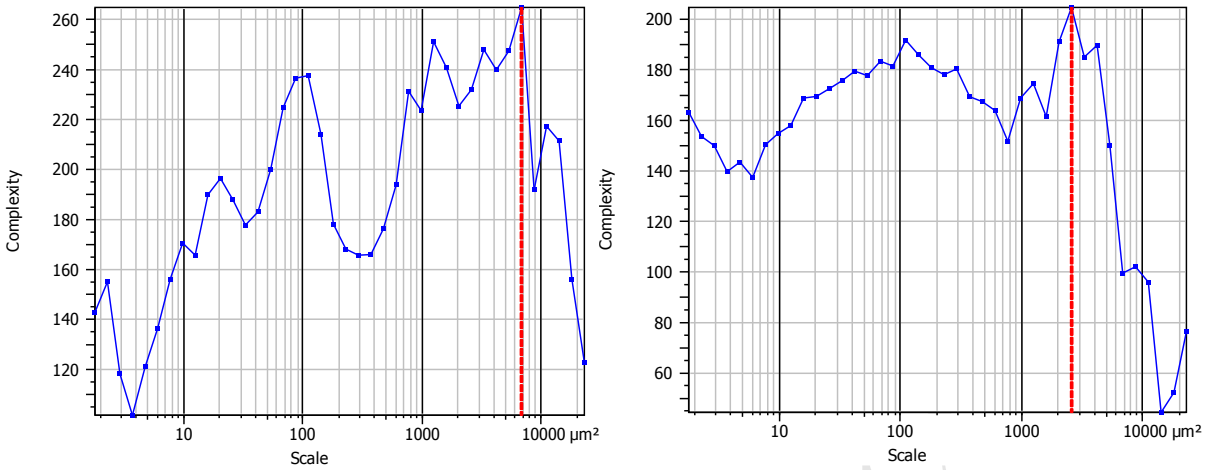

Fig. 8 Analytical domain of luminance scale sensitivity analysis of (a) complexity scale area of one corner of the resins sample (b) complexity of four corner methodology of the resins sample

The analytical domain of the scale of sensitivity analysis and the regression settings of the system was also done automatically for the length scale columns, analytical method at a SRC threshold of the same 10% of the resins sample which is shown in Fig. 9 A area scale of length scale columns methodology was used of a SRC of 192µm² and a bigger SRC threshold of 9736 compared to others. It has a fractal complexity of 1.71 on the same number of point 200 as that of one corner methodology. It has a fractional dimension of 2.38 with a maximum scale complexity of 215µm. The regression coefficient of the 'R' square equation is 0.788 and the regression line intercept at 'Y axis' is 3.99 with a regression slope of -0.00172 as shown in Fig. 9.

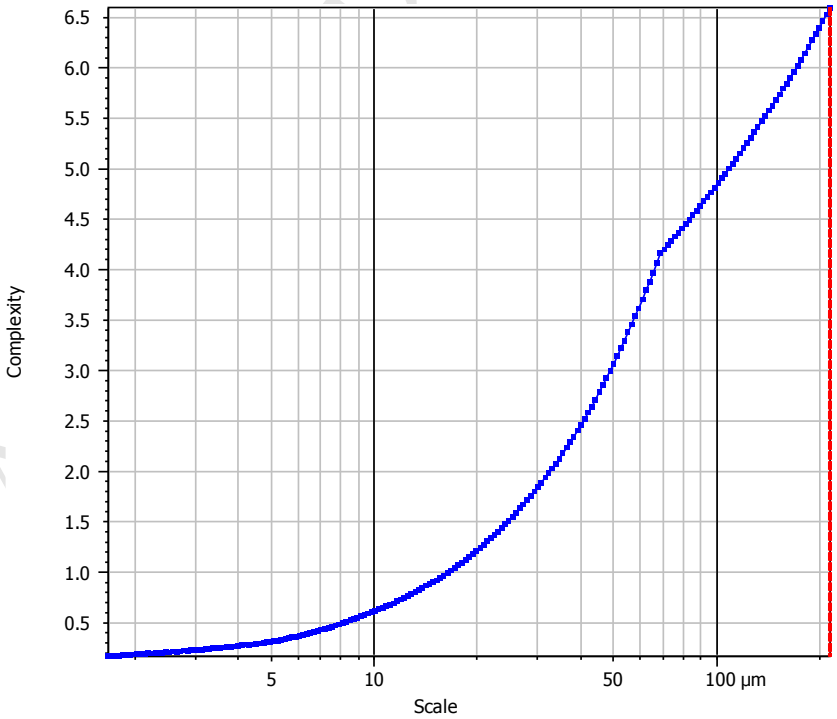

Fig. 9. Scale sensitivity analysis of the specimen of complex scale length columns

Analysing the graph as a whole, it was noticed that this polymer has a semi-crystalline behaviour indicating that it has a moderate molecular weight, its behaviour indicates that the resin presents characteristics similar to commercial polyurea. The remarkable change of phase with mass gain until reaching an exothermic peak around 150°C, this phenomenon is related to the primary crystallization of the resin in question, in this phase, the polymer presents glassy behaviour. The baseline change without peak around 150°C to approximately 280°C indicates that in this temperature range the material shows a rubbery behaviour between Tg and Tm [39]. The strong exothermic peak identified after 300^{o}C to 500^{o}C with a consequent mass gain indicates the occurrence of a secondary crystallization of this polymer, so its behaviour at this temperature range is rubbery. Finally, upon reaching 500°C the material reaches its melting temperature. Analyzing the curve as a whole, this material shows a behaviour of a semi-crystalline polymer, with characteristics similar to those of the commercially available polyester. The remarkable mass loss from initial heating to approximately 90°C exhibiting a strong endothermic peak identified at 90°C, in that temperature range the polymer exhibits vitreous behaviour [40]. After 90°C due to phase change with consequent mass gain and the presence of several exothermic peaks, a primary crystallization occurs, reaching a temperature of up to 300°C. In this temperature range, the polymer shows a rubbery behaviour [41]. In addition, after 300°C there is still a new and larger mass gain with a new baseline change, indicating the occurrence of a secondary crystallization with the presence of an exothermic peak extending to 500°C, at this stage the polymer has a still rubbery behaviour. Finally, around 500°C, the presence of an endothermic peak and a new baseline change are noted, indicating that the material has reached its melting temperature. In general, when analysing this material, it is noted that it presents the behaviour of a semicrystalline polymer, with characteristics similar to the commercial polyurea. According to the promising results obtained in this study, it is now necessary to evaluate the three-dimensional printing of these materials properly, using numerical control and automated control parameters, in an attempt to manufacture different objects. In addition, the investigation of the application of other plant resins obtained from other species of trees, intended for use in 3D printing is also made substantially necessary due to the innumerable species of trees in the world

4. Conclusion

The evaluated materials presented similar characteristics among themselves, being able to be extruded in the elaboration of filaments, aiming consequently to use in ADT impression, using the technique of modelling by fuse deposition. The aim of this study was to propose a novel investigation for possible reinforcement of different resins and examine it nanoparticles and microstructural behaviour to enhance productivities of ADM. According to the results obtained in the tensile and compression tests, the resistance of the polymers was low when compared to the other commercial plastics, but they presented adequate values if the desired application were treated. According to the results obtained in differential scanning calorimetry and the analysis of the microstructure. The resins showed different behaviour from the low-temperature state to the high-temperature state which is typical of crystalline and semicrystalline polymers, with characteristics similar to the polyurea and polyester commercial plastics. The resins presented different thermoplastic behaviour. As a suggestion for future work, it is suggested to investigate values concerning the contraction and expansion of these materials, as well as their biodegradability and emissions of

compounds when subjected to heating processes, such as those occurring in the cast - deposition. In addition, this study opens the way for other researches regarding the identification of the characteristics of other vegetable resins available for application in 3D printing. It can also be observed that resin B give a higher tensile and compressive force of about 365KN/m^2 and 650KN/m^2 respectively comparable to others. The optimum values for resins A and C at a ductile state for both the tensile and compressive force is at 170KN/m^2 and 300KN/m^2 respectively.

5. References

[1] Boschetto A, Giordano V, Veniali F, "3D roughness profile model in fused deposition modelling," *Rapid Prototyp J,* vol. 19, p. 240–52, 2013.

[2] S. Berretta, K. Evans, O. Ghita, "Additive manufacture of PEEK cranial implants: Manufacturing considerations versus accuracy and mechanical performance," *Materials and Design,* vol. 139, p. 141–152, 2018.

[3] Gaoyan Zhonga, Mohammad Vaezi, Ping Liu, Lin Pand, Shoufeng Yang, "Characterization approach on the extrusion process of bioceramics for the 3D printing of bone tissue engineering scaffolds," *Ceramics International,* vol. 43, p. 13860–13868, 2017.

[4] Lijun Deng, Yi Deng, Kenan Xie,, "AgNPs-decorated 3D printed PEEK implant for infection control and bone repair," *Colloids and Surfaces B: Biointerfaces,* vol. 160, p. 483–492, 2017.

[5] Antonelli, M., Knudson, I., Popernack, A., Schuler, A.,, "Cast aluminummesostructures using 3D printed sand cores with an encapsulation," *Int. J.Metal cast,* vol. 10, no. 1, p. 111–113, 2016.

[6] Ang, S.F., Bortel, E.L., Swain, M.V., Klocke, A., Schneider, G.A.,, "Size-dependent elastic/inelastic behavior of enamel over millimeter and nanometer length scales," *Biomaterials,* vol. 31, no. 7, p. 1955–1963, 2010.

[7] Armstrong, S., Geraldeli, S., Maia, R., Raposo, L.H., Soares, C.J., Yamagawa, J.,, "Adhesion to tooth structure: a critical review of ‘‘micro’’ bond strength test methods," *Dental Materials,* vol. 26, no. 2, p. 50–62., 2010.

[8] Farzad Liravi, Mihaela Vlasea, “Powder bed binder jetting additive manufacturing of silicone structures”.

[9] De Munck, J., Mine, A., Poitevin, A., Van Ende, A., Cardoso, M.V., Van Landuyt, K.L., Peumans, M., Van Meerbeek, B.,, "Meta- analytical review of parameters involved in dentin bonding.," *Journal of Dental Research,* vol. 91, no. 4, p. 351–357, 2012.

[10] Atai, M., Pahlavan, A., Moin, N.,, "Nano-porous thermally sintered nano silica as novel fillers for dental composites," *Dent. Mater,* vol. 2012, p. 133–145., 28.

[11] Balos, S., Pilić, B., Petronijević, B., Marković, D., Mirković, S., Sarcev, I.,, "Improving mechanical properties of flowable dental composite resin by adding silica nanoparticles.," *Vojnosanit. Pregl.,* vol. 70, p. 477–483., 2013.

[12] Zadeh MH, Mirzaee O, Saidi P, "Structural and mechanical characterization of Al-based composite reinforced with heat treated Al2O3 particles," *Mater Des,* vol. 54, p. 245–50, 2014.

[13] Kimura, F., Kadoya, S., Kajihara, Y.,, "Effects of molding conditions on injection molded direct joining using a metal with nano-structured surface," *Precis. Eng.,* vol. 45, p. 203–208., 2016.

[14] Boschetto A, Bottini L, Veniali F, "Microremoval modelling of surface roughness in barrel finishing," *Int J Adv Manufact Technol,* vol. 69, p. 2343–54, 2013.

[15] Magni, E., Ferrari, M., Hickel, R., Ilie, N.,, "Evaluation of the mechanical properties of dental adhesives and glass-ionomer cements," *Clinical Oral Investigations,* vol. 14, no. 1, p. 79–87, 2010.

[16] Hiba Bargaoui, Farida Azzouz, Delphine Thibault, Georges Cailletaud, "Thermomechanical behavior of resin bonded foundry sand coresduring casting," *Journal of Materials Processing Technology,* vol. 246, p. 30–41, 2017.

[17] Heba A. El-Deeb, Radwa M. Ghalab, Mai M. Elsayed Akah, Enas H. Mobarak,, "Repair bond strength of dual-cured resin composite core buildup materials,," *Journal of Advanced Research,* vol. 7, p. 263–269., 2016.

[18] P. Withers, "Fracture mechanics by three-dimensional crack-tip synchrotron Xray microscopy," *Philos. Trans. A Math. Phys. Eng. Sci.,* vol. 373, no. 6, pp. 2013-157, 2015.

[19] Wei Zhang, Chase Cotton, Jessica Sun, Dirk Heider, Bohong Gu, Baozhong Sun, Tsu-Wei Chou,, "Interfacial bonding strength of short carbon fiber/acrylonitrile-butadienestyrene composites fabricated by fused deposition modeling," *Composites Part B,* vol. 137, p. 51–59, 2018.

[20] Sajjdi SA, Ezatpour HR, Parizi MT, "Comparison of microstructure and mechanical properties of A356 aluminum alloy/Al2O3 composites fabricated by stir and compo-casting processes," *Mater Des,* vol. 34, p. 106–11, 2012.

[21] J.K. Watson, K.M.B. Taminger, “A decision-support model for selecting additive manufacturing versus subtractive manufacturing based on energy consumption,” *Journal of Cleaner Production,* vol. 176, pp. 1316-1322, 2018.

[22] Mobarak E, El-Deeb H., "Two-year interfacial bond durability and nanoleakage of repaired silorane-

based resin composite," *Oper Dent,* vol. 38, p. 408–18., 2013.

[23] Rathke A, Balz U, Muche R, Haller B., "Effects of self-curing activator and curing protocol on the bond strength of composite core buildups," *J Adhes Dent,* vol. 14, p. 39–46., 2016.

[24] Opdam NJ, Bronkhorst EM, Loomans BA, Huysmans MC., "Longevity of repaired restorations: a practice based study," *J Dent,* vol. 40, p. 829–35., 2012.

[25] S. Singha, R. Singh, "Development of functionally graded material by fused deposition modelling assisted investment casting," *Journal of Manufacturing Processes,* vol. 24, p. 38–45, 2016.

[26] Singh R, Singh S, "Effect of process parameters on surface hardness, dimensional accuracy and surface roughness of investment cast components," *J Mech Sci Technol,* vol. 27, p. 191–7, 2013.

[27] El-Askary FS, El-Banna AH, "van Noort R. Immediate vs delayed repair bond strength of a nanohybrid resin composite.," *J Adhes Dent,* vol. 14, p. 265–74, 2012.

[28] F. Liravi, E. Toyserkani, "A hybrid additive manufacturing method for the fabrication of silicone bio-structures: 3D printing optimization and surface characterization," *Mater Des,* vol. 138, pp. 46-61, 2017.

[29] Asuka Suzuki, Yuta Arai, Naoki Takata, Makoto Kobashi, "Effect of layer thickness on bonding strength of Al/epoxy resin joints via interpenetrating phase layer,," *Journal of Materials Processing Tech,* vol. 254, p. 338–345, 2018.

[30] Berto, F., Elices, M., Lazzarin, P., Zappalorto, M.,, "Fracture behaviour of notched round bars made of PMMA subjected to torsion at room temperature.," *Eng. Fract. Mech.,* vol. 90, p. 143–160., 2012.

[31] Sithiprumnea Dul, Luca Fambri, Alessandro Pegoretti, "Fused deposition modelling with ABS–graphene nanocomposites," *Composites: Part A,* vol. 85, p. 181–191, 2016.

[32] D.P. Schmitz, L.G. Ecco, S. Dul, E.C.L. Pereira, B.G. Soares, G.M.O. Barra, A. Pegoretti, "Electromagnetic interference shielding effectiveness of ABS carbon-based composites manufactured via fused deposition modelling," *Materials Today Communications,* vol. 15, p. 70–80, 2018.

[33] Liu, Y., Tja¨derhane, L., Breschi, L., Mazzoni, A., Li, N., Mao, J., Pashley, D.H., Tay, F.R.,, "Limitations in bonding to dentin and experimental strategies to prevent bond degradation.," *Journal of Dental Research,* vol. 90, no. 8, p. 953–968., 2011.

[34] Mobin Yahyazadehfar, Mustafa MuratMutluay, Hessam Majd, Heonjune Ryou, Dwayne Arola, "Fatigue of the resin–enamel bonded interface and the mechanisms of failure," *j o u r n a l o f t h e m e c h a n i c a l b e h a v i o r o f b i o m e d i c a l m a t e r i a l s,* vol. 21, p. 1 2 1 – 1 3 2, 2013.

[35] J. S. Chohana, R. Singhb, K. S. Boparai, “Mathematical modelling of surface roughness for vapour processing of ABS parts fabricated with fused deposition modeling,” *Journal of Manufacturing Processes,* vol. 24, p. 161–169, 2016.

[36] Boschetto A, Bottini L, “Roughness prediction in coupled operations of fused deposition modelling and barrel finishing,” *J Mater Process Technol,* vol. 219, p. 181–92, 2015.

[37] Balos, S., Pilic, B., Markovic, D., Pavlicevic, J., Luzanin, O.,, "Poly(methylmethacrylate) nanocomposites with low silica addition," *. J. Prosthet. Dent.,* vol. 111, p. 327–334., 2014.

[38] Heba A. El-Deeb, Sara Abd El-Aziz, Enas H., "Mobarak Effect of preheating of low shrinking resin composite on intrapulpal temperature and microtensile bond strength to dentin," *Journal of Advanced Research,* vol. 6, p. 471–478, 2015.

[39] Stojanović, D.B., Brajović, L., Orlović, A., Dramlić, D., Radmilović, V., Uskoković, P.S., Aleksić, R.,, "Transparent PMMA/silica nanocomposites containing silica," *Prog. Organ Coat,* vol. 76, p. 626–631., 2013.

[40] Kazuaki Katagiri, Katsuhiko Sasaki, Shinya Honda, Hikaru Nakashima, Yusuke Tomizawa,, "Resin molding by using electro-activated deposition for efficient manufacturing of carbon fiber reinforced plastic," *Composite Structures,* vol. 182, p. 666–673, 2017.

[41] Marianthi Topouzi, Eleana Kontonasaki, Dimitrios Bikiaris, Lambrini Papadopoulou, Konstantinos M. Paraskevopoulos, Petros Koidis, "Reinforcement of a PMMA resin for interim fixed prostheses with silica nanoparticles,," *Journal of the mechanical behavior of biomedical materials,* vol. 69, p. 213–222, 2017.